JOURNAL OF GUIDANCE, CONTROL, AND DYNAMICS
Vol. 23, No. 1, January–February 2000

Space-Based Visible Data Reduction

J. Sharma,* C. von Braun,† and E. M. Gaposchkin‡
Lincoln Laboratory, Massachusetts Institute of Technology, Lexington, Massachusetts 02420

The Midcourse Space Experiment satellite, launched 24 April 1996, carries the Space-Based Visible (SBV) sensor package designed for conducting space surveillance from a space platform. The SBV sensor consists of a visible imaging charged couple device sensor that generates sets of images of resident space objects against a star background. These images are either directly sent to a tape recorder for later transmission to the ground for processing, or more commonly, they are processed onboard the sensor package and only the data associated with the stars and potential resident space objects are downlinked for processing. The SBV data reduction process of generating metric observations from SBV data is described. This process consists of first determining an accurate pointing of the SBV sensor using the star background. The refined pointing is then used to generate right ascension and declination observations for the resident space object. Finally, the resident space objects are identified by correlating the observations with a complete resident space object catalog. The algorithms used are discussed, and a summary of data processed is presented.

Nomenclature

(a_{ij}^{nm})	= distortion model coefficients
$\boldsymbol{R}_1, \boldsymbol{R}_2, \boldsymbol{R}_3$	= rotation matrices about (x, y, z) Midcourse Space Experiment body-fixed axes, respectively
(z, y)	= measured centroid focal plane coordinates
(z_0, y_0)	= offsets in the borsight
$(\tilde{z}, \tilde{y})$	= focal plane coordinates with offsets
(α^*, δ^*)	= star catalog position
$(\alpha_0, \delta_0, \psi_0)$	= a priori right ascension, declination, and roll angle of Space-Based Visible borsight
(ζ, η)	= focal plane coordinates with optical distortion
(θ)	= offset in roll angle

Introduction

THE application of electro-optical technology to the tracking of resident space objects (RSOs) was developed at the Massachusetts Institute of Technology Lincoln Laboratory in the late 1970s and resulted in the deployment of the Ground-Based Electro-Optical Deep-Space Surveillance (GEODSS) system by the U.S. Air Force. The system consists of multiple 1.0-m f/2.15 folded Newtonian telescopes with a 2-deg field of view. The detector used is a Westinghouse intensified electron-bombarded silicon diode array camera (I-Ebsicon). Similar to Space-Based Visible (SBV) data reduction, a detection on the Ebsicon focal is converted to right ascension and declination by knowing where the telescope is pointed. The pointing of the ground-based GEODSS camera is determined by modeling the mount of the telescope. The model of mount is routinely calibrated by observing stars with well-defined positions.[1] In SBV data reduction, the boresight pointing is determined for each detection of an RSO by matching the detected stars to a star catalog. Finally, SBV is located on an orbiting platform and its position must be estimated from tracking data for the Midcourse Space Experiment (MSX).

The goal of SBV is to demonstrate the ability to make observations of RSOs from a space-based platform. This paper describes how these data are reduced to generate metric observations of RSOs. The SBV sensor is a 15-cm-aperture off-axis, reimaging, all-reflective telescope with a thermoelectrically cooled, bare charge-coupled-device (CCD) focal plane. Also contained onboard the MSX spacecraft is a signal processor and supporting electronics. The SBV focal plane consists of four three-sided abuttable frame transfer CCDs, each composed of 420 × 420, 27-μm pixels. Additional characteristics of the SBV are presented in Table 1 (Ref. 2).

The principal task for SBV is to perform space surveillance. There are two tracking modes that are employed to observe RSOs. The most commonly used method is to track the background stars so they appear as pointlike sources on the focal plane. All RSOs will have a relative motion with respect to stars and will appear as streaks on the focal plane. This first method is known as sidereal tracking. The second method is to track the RSO such that it appears as a point source on the focal plane, and the stars appear as streaks on the focal plane. The method is called ephemeris track mode. Any additional RSOs that are in the SBV's field of view and are not being tracked will also appear as streaks on the focal plane in the ephemeris track mode.

Data Processing

The data flow for SBV is shown in Fig. 1. A typical observation of an RSO by SBV consists of 6–16 420 × 420 pixel frames. These frames can be downlinked as raw images via an onboard tape recorder. A second option is to process all of the frames through the onboard signal processor. The SBV signal processor extracts the pertinent information from the raw frames, which are then downlinked as a signal processor report. The report contains data on focal plane detections in the frame set that appear as point sources and those that appear as streaks. The most significant advantage of using the signal processor is the reduction by two orders of magnitude in the amount of information that has to downlinked. For 16 420 × 420 frames, 5000 kB of raw image data are reduced to 3 kB. The onboard processing allows more data to be returned from the spacecraft in a timely fashion. The signal processor is primarily used to process observations using the sidereal tracking mode, which constitutes the primary method of observing RSOs.

Figure 2 shows examples of the different data types and the two different tracking modes. Both tracking methods are performed in an open-loop mode. A description of the examples is summarized in Table 2. Figures 2a and 2b represent a special data-take mode, where both the raw frames and signal-processed frames are sent to the ground. Figure 2b is a reconstructed image of the signal processor report file. This image shows the square blocks (7 × 7 pixels), representing detections that the signal processor labels as star candidates. The number of star candidates desired must be specified to the signal processor, and the number was set to 20 for this observation. The streak detection is also plotted and consists of a 5-pixel-wide region that the signal processor labels as a streak candidate. Figure 2c represents data taken using the ephemeris track mode in which two

Received 16 November 1998; revision received 12 July 1999; accepted for publication 3 August 1999.

*Technical Staff Member, Surveillance Techniques Group.

†Technical Staff Member and Midcourse Space Experiment Surveillance Principal Investigator; currently Assistant Group Leader and Midcourse Space Experiment Surveillance Principal Investigator.

‡Senior Staff Member (retired) and former Midcourse Space Experiment Surveillance Principal Investigator.

satellites were identified, one that was being tracked and another that appeared coincidentally. Once the image has been processed through either the onboard or ground processor and the star and streaklike detections have been identified, the next step is to perform metric reduction on the data. A flow diagram of the processing is presented in Fig. 3.

The SBV is a self-calibrating sensor, in that it determines the boresight pointing from the data it collects. This is accomplished by matching the detected stars to catalog star positions. This matching is performed on the focal plane and requires the mapping of catalog stars onto the focal plane. The SBV has highly distorted optics (not diffraction limited) due to its design that maximizes the rejection of stray light from the focal plane. This distortion must be accurately modeled for the star matching procedure to work. The mapping of catalog stars to the focal plane is a two-step process. The convention for the focal plane adopted here is the mapping of the MSX spacecraft body-fixed axis on to the focal plane and is shown in Figs. 4 and 5, respectively. The first step involves the mapping the catalog stars to an undistorted focal plane position (z, y):

$$\begin{bmatrix} 1 \\ y/P_{\text{scale}} \\ z/P_{\text{scale}} \end{bmatrix} = \boldsymbol{R}_1(\psi_0)\boldsymbol{R}_2(-\delta_0)\boldsymbol{R}_3(\alpha_0) \begin{bmatrix} \cos\alpha^* \cos\delta^* \\ \sin\alpha^* \cos\delta^* \\ \sin\delta^* \end{bmatrix} \quad (1)$$

Assuming 12.5 arc-s/pixel, the plate scale is

$$P_{\text{scale}} = 1/\sin(12.5/3600) = 16501.185$$

Table 1 SBV characteristics

Property	Value
Spectral range	0.3–0.9 μm
Spatial resolution	12.1 arc-s/pixel
Field of view	1.4 ×6.6 deg
Aperture, f-number	15 cm, f/3
Frame integration times	0.4, 0.5, 0.625, 1.0, 1.6, 3.12 s
Frame sizes	420 ×420, 357 ×420, 178 ×420 pixels
Dynamic range	12 bit
Quantum efficiency	28%

Table 2 Description summary

Data	Fig. 2a	Fig. 2b	Fig. 2c
Image type	Raw	Signal-processed report	Raw
Tracking mode	Sidereal	Sidereal	Ephemeris
Number of frames	16	16	16
Frame integration	0.625 s	0.625 s	1 s
Time correlated object	Lageos II	Lageos II	GPS IIA-13, Cosmos, debris
Image size, pixels	420 ×420	420 ×420	357 ×420

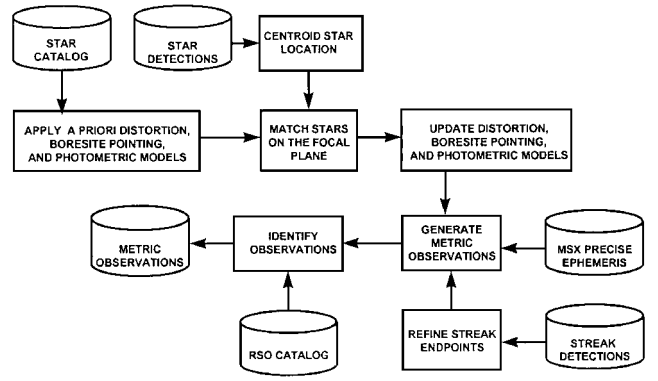

Fig. 3 SBV metric data reduction.

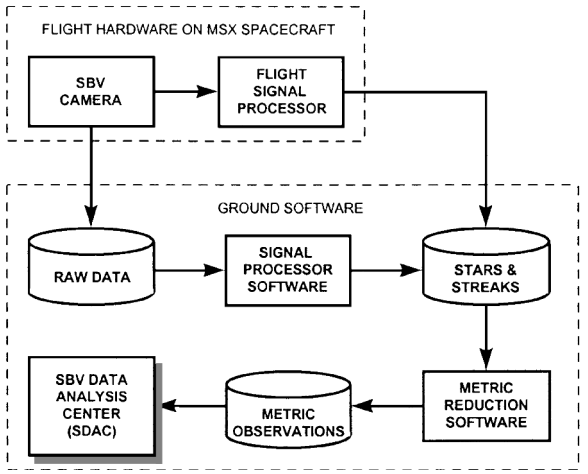

Fig. 1 SBV data flow diagram.

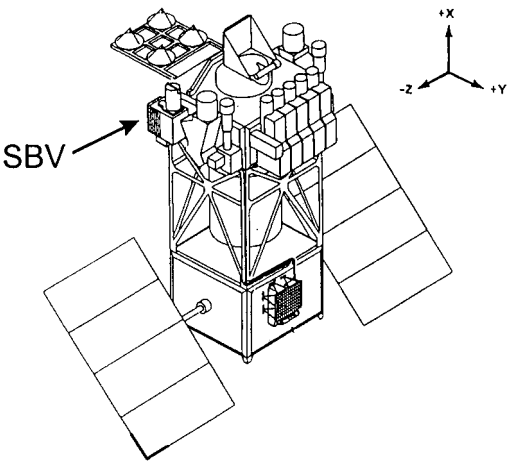

Fig. 4 MSX spacecraft body-fixed axes.

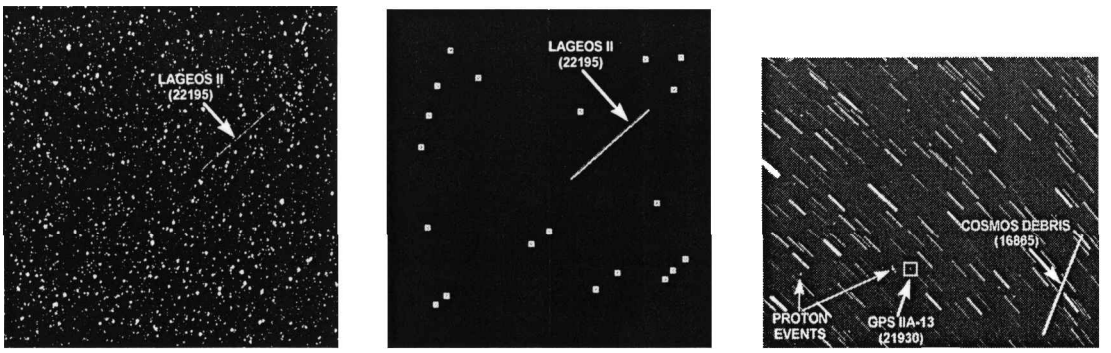

a) b) c)

Fig. 2 Examples of SBV data.

The next step in transforming the undistorted focal plane coordinates into distorted focal plane coordinates is to account for offsets in the boresight (z_0, y_0) and an error in roll angle (θ):

$$\begin{bmatrix} \zeta \\ \eta \end{bmatrix} = \begin{bmatrix} \cos\theta & \sin\theta \\ -\sin\theta & \cos\theta \end{bmatrix} \begin{bmatrix} z - z_0 \\ y - y_0 \end{bmatrix} \tag{2}$$

The final transformation is the application of the distortion model to generate distorted focal plane coordinates $(\tilde{z}, \tilde{y})$:

$$\begin{bmatrix} \tilde{z} \\ \tilde{y} \end{bmatrix} = \boldsymbol{A} \begin{bmatrix} \zeta \\ \eta \end{bmatrix} \tag{3}$$

$$\boldsymbol{A} = \begin{bmatrix} a_{11} & a_{12} \\ a_{21} & a_{22} \end{bmatrix} \tag{4}$$

$$\begin{aligned} a_{11} &= a_{11}^{00} + a_{11}^{10}\zeta + a_{11}^{01}\eta + a_{11}^{20}\zeta^2 + a_{11}^{11}\zeta\eta + a_{11}^{02}\eta^2 \\ a_{21} &= a_{21}^{00} + a_{21}^{10}\zeta + a_{21}^{01}\eta + a_{21}^{20}\zeta^2 + a_{21}^{11}\zeta\eta + a_{21}^{02}\eta^2 \qquad a_{12} = a_{21} \\ a_{22} &= a_{22}^{00} + a_{22}^{10}\zeta + a_{22}^{01}\eta + a_{22}^{20}\zeta^2 + a_{22}^{11}\zeta\eta + a_{22}^{02}\eta^2 \end{aligned} \tag{5}$$

Figure 6 is an illustration of the distortion that is present. Figure 6 shows the star detections from actual SBV observations. The distortion model coefficients (a_{ij}^{nm}) have been determined from analysis of on-orbit data taken in dense star fields. Figure 6 shows the position of distorted and undistorted detection locations for CCD3 and CCD1. The distortion is on the order of tens of pixels for CCD3 and increases to more than 100 pixels on CCD1.

The star matching consists of matching the coordinates $(\tilde{z}, \tilde{y})$ to the centroid locations of the star detections (z, y). The centroid location is calculated by fitting a point spread function to each detection to minimize errors from the detection of apparent and partial double stars. The matching process involves two steps. The first step consists of a coarse star match that involves matching a pattern of lines and vertices connecting a few selected stars and is intended to account for initial pointing errors. Once the first step has succeeded, the next step is a more precise star matching procedure that involves comparing the (z, y) pixel locations of detected and catalog stars. The difference of the two star positions is used to drive a least-squares operation that updates the SBV attitude by adjusting the parameters $(z_0, x_0, \theta, a_{11}^{00}, a_{22}^{00})$. The remaining terms in the distortion model are not estimated for each data set. The final matching process is iterated until the number of matched stars does not increase. The matched stars are also used to update the magnitude offset term (V_0). This offset is used to convert the detected intensity to a SBV magnitude:

$$\text{SBV magnitude} = -2.5\log\left(\frac{\text{total intensity}}{\text{total integration time}}\right) + V_0 \tag{6}$$

The final step in updating the SBV attitude requires converting (z_0, x_0, θ) to an updated attitude (α, δ, ψ). The right ascension (RA) and declination (DEC) are calculated using the following relationship:

$$\begin{aligned} &\begin{bmatrix} \cos\alpha\cos\delta \\ \sin\alpha\cos\delta \\ \sin\delta \end{bmatrix} \\ &= \boldsymbol{R}_3(-\alpha_0)\boldsymbol{R}_2(\delta_0)R_1(-\psi_0) \begin{bmatrix} \sqrt{1 - (y_0/P_{\text{scale}})^2 - (z_0/P_{\text{scale}})^2} \\ y_0/P_{\text{scale}} \\ z_0/P_{\text{scale}} \end{bmatrix} \\ &= \hat{l}_1 \end{aligned} \tag{7}$$

Updating the roll angle is slightly more complex and is described as

$$\tan\psi = \hat{l}\cdot\hat{l}_3/\hat{l}\cdot\hat{l}_2 \tag{8}$$

where

$$\hat{l} = \boldsymbol{R}_3(-\alpha_0)\boldsymbol{R}_2(\delta_0) \begin{bmatrix} 0 \\ \cos(\psi + \theta) \\ \sin(\psi + \theta) \end{bmatrix} \tag{9}$$

and

$$\hat{l}_2 = \begin{bmatrix} 0 \\ 0 \\ 1 \end{bmatrix} \times \hat{l}_1, \qquad \hat{l}_3 = \hat{l}_1 \times \hat{l}_2 \tag{10}$$

Once the attitude has been updated, the next step is to refine the streak endpoints using the signature information that is sent down with the streak. The signature data, generated by the signal processor, is a 5-pixel-wide swath that encompasses the streak and consists of the maximum minus the mean intensity of the streak pixels and the frame in which it occurs. The signature allows the data reduction process to overcome two limitations of the signal processor:

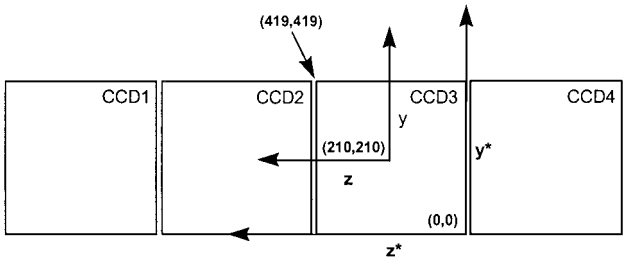

Fig. 5 Focal plane coordinates with *x* axis directed out of the paper.

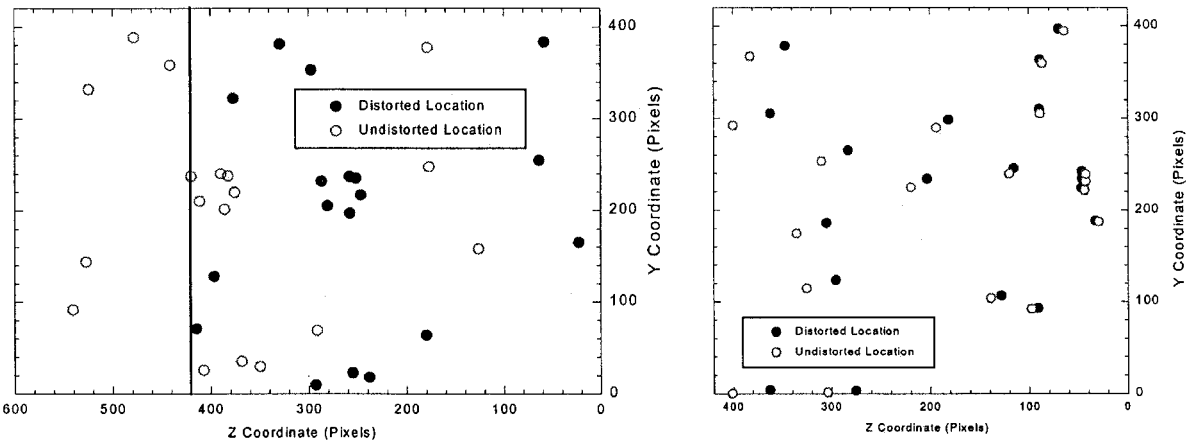

CCD1 **CCD3**

Fig. 6 SBV distortion.

1) Integer arithmetic limits the accuracy of endpoint calculations to one pixel. 2) The signal processor is unable to screen out bad pixels. The refinement process consists of throwing out bad pixels not belonging to the time continuum of the streak and of fitting a line through the signature data. The endpoints of the line are taken as the refined endpoints. Once the endpoints have been determined, they must be transformed from focal plane coordinates to object space coordinates (RA, DEC). The streak endpoints must first be transformed from distorted to undistorted focal plane coordinates. This step requires the inversion of the distortion model and is an iterative process due to its nonlinearity. The following expression is iterated to calculate the undistorted focal plane location (ζ, η) of the detection:

$$\begin{bmatrix} \zeta_{n+1} \\ \eta_{n+1} \end{bmatrix} = \boldsymbol{A}^{-1}(\zeta_n, \eta_n) \begin{bmatrix} \tilde{z} \\ \tilde{y} \end{bmatrix} \tag{11}$$

using the following initial condition:

$$\begin{bmatrix} \zeta_0 \\ \eta_0 \end{bmatrix} = \begin{bmatrix} \tilde{z} \\ \tilde{y} \end{bmatrix} \tag{12}$$

$$\begin{bmatrix} z \\ y \end{bmatrix} = \begin{bmatrix} \cos(-\theta) & \sin(-\theta) \\ -\sin(-\theta) & \cos(-\theta) \end{bmatrix} \begin{bmatrix} \zeta \\ \eta \end{bmatrix} + \begin{bmatrix} z_0 \\ y_0 \end{bmatrix} \tag{13}$$

$$\begin{bmatrix} \cos\bar{\alpha}\cos\bar{\delta} \\ \sin\bar{\alpha}\cos\bar{\delta} \\ \sin\bar{\delta} \end{bmatrix} = \boldsymbol{R}_3(-\alpha_0)\boldsymbol{R}_2(\delta_0)\boldsymbol{R}_1(-\psi_0) \times \begin{bmatrix} \sqrt{1-(y/P_{\text{scale}})^2-(z/P_{\text{scale}})^2} \\ y/P_{\text{scale}} \\ z/P_{\text{scale}} \end{bmatrix} \tag{14}$$

where $(\bar{\alpha}, \bar{\delta})$ are the streak endpoint positions (RA and DEC).

After the RA and DEC locations of the streak endpoints are calculated, two observations are formed by attaching the precise location of MSX in World Geodetic System-84 Earth-fixed coordinates to each observation.[3] Once the observations have been formed, it is necessary to identify the observations. This is accomplished by taking a complete catalog of RSOs and propagating each of the orbital element sets to the observation's time and by comparing the predicted RSO position to the observation. In practice the performance of the correlation process is increased by first performing a coarse correlation by propagating all of the RSOs using a simple propagation model (two-body plus second order zonal spherical harmonic geopotentional terms). Only RSOs that pass through the first filter are then propagated again using a more precise ANODE model (two-body, second, third, and fourth order zonal spherical harmonic geopotential terms, sun, and moon).[4] Once identified, the observations are available for orbit processing and further assessment.

Processing Results

This section describes the processing results of 11,300 onboard signal-processed data sets. This data was taken during the first year of operation of the SBV between May 1996 and November 1997. CCD3 has collected 70% of the data, with the remaining data equally divided among the other three CCDs. No degradation of performance has been observed among the CCDs. The distortion model coefficients were calculated with onboard data collected during the first several weeks of SBV operation.[5] The goal of this section is to describe the current performance of the SBV surveillance data processing. The results for the star matching process are based on the use of the Astrographic Catalog, which has the lowest systematic errors of currently available catalogs at 0.2 arc-s for the majority of stars in the catalog.[6] The star positions used are in $J2000$ inertial frame. It contains approximately 320,000 stars down to a visual magnitude of 10.5. The distribution of the number of stars matched for each data set is shown in Fig. 7 and shows that on average 11 stars are matched. The quality of the star matches currently being achieved is shown in Fig. 8. Figure 8 shows the distribution of the rms star-fit residuals over all of the data sets and indicates the quality of the average star match. The tightness of the results indicates that there are no significant variations in the distortion model coefficients and that it is sufficient to estimate only the linear terms in the distortion model $(a_{11}^{00}, a_{22}^{00})$.

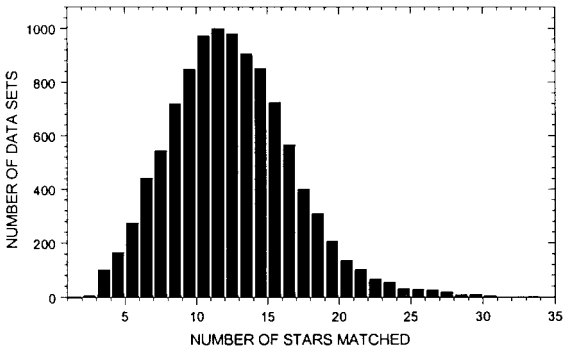

Fig. 7 Number of star matches per frameset.

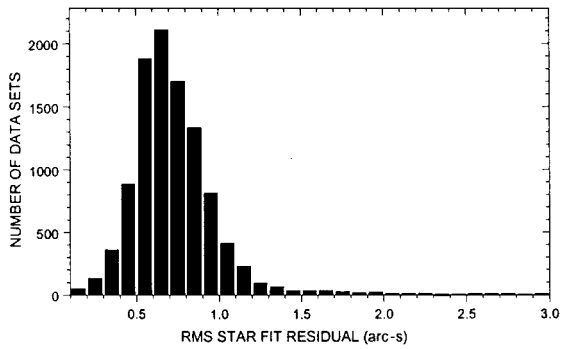

Fig. 8 RMS star-fit residual per frameset.

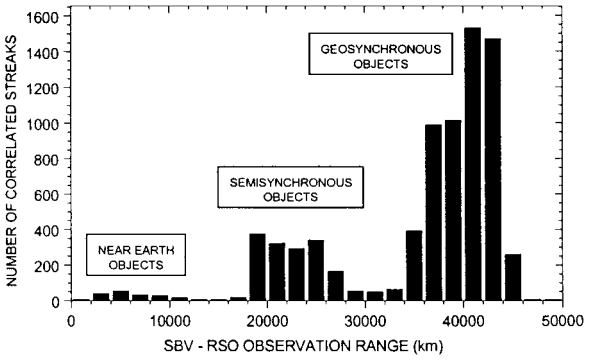

Fig. 9 Categories of objects observed.

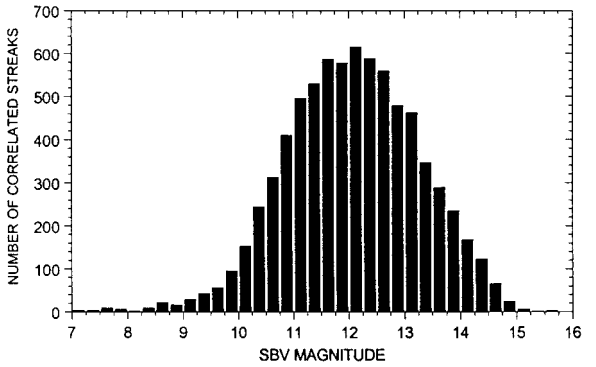

Fig. 10 SBV magnitude of correlated objects.

Figures 7 and 8 can also be used to approximate the uncertainty of the estimated boresight for each data set. Because the boresight is estimated using a least-squares process, an estimate of uncertainty in the boresight can be approximated by scaling the rms star-fit residuals by the square root of the number of matched stars used in the fitting process. This approximation implies a boresight pointing

uncertainty of a few tenths of an arc-s, which approaches the accuracy of current star catalogs. Over 6100 signatures have been correlated. The distribution of SBV–RSO ranges is shown in Fig. 9. SBV primarily observes deep space objects, and the two broad categories that were observed are indicated in Fig. 9. Objects in geotransfer orbits may appear in both semisynchronous and geosychronous categories. The estimated magnitude of these observations is plotted in the Fig. 10. Figure 10 shows that detections down to 14th magnitude are routinely correlated.

Conclusion

The SBV instrument on the MSX has successfully collected over 11,000 frame sets of space surveillance data. These data have been successfully processed through the metric data reduction software. The distortion model has been accurately realized and has produced subarc-s star matches over the first 18 months of the mission. Observations, to date, have been correlated on over 6000 RSOs as dim as 15th magnitude.

References

[1] Pearce, E. C., "Electro-Optical Deep-Space Tracking," *Proceedings of the Third US/Russian Space Surveillance Workshop*, U.S. Naval Observatory, Washington, DC, Oct. 1998, pp. 15–25.

[2] Mill, J. D., O'Neil, R. R., Price, S., Romick, G. J., Uy, O. M., and Gaposchkin, E. M., "Midcourse Space Experiment: Introduction to the Spacecraft, Instruments, and Scientific Objectives," *Journal of Spacecraft and Rockets*, Vol. 31, No. 5, 1994, pp. 900–907.

[3] Abbot, R. I., von Braun, C., and Gaposchkin, E. M., "Midcourse Space Experiment Precision Ephemeris," *Journal of Guidance, Control, and Dynamics*, Vol. 23, No. 1, 2000, pp. 187–191.

[4] Lane, M. T., "On Analytic Modeling of Lunar Perturbations of Artificial Satellites of the Earth," Lincoln Lab. TR 841, Massachusetts Inst. of Technology, Lexington, MA, June 1989.

[5] von Braun, C., Sharma, J., and Gaposchkin, E. M., "Space-Based Visible Metric Accuracy," *Journal of Guidance, Control, and Dynamics*, Vol. 23, No. 1, 2000, pp. 176–182.

[6] Corbin, T. E., and Urban, S. E., "Astrographic Catalogue Reference Stars (Documentation for the Computer-Readable Version)," Doc. NSSDC/WDC-A-R&S 91-10, National Space Science Data Center, 1991.